Artificial water channels-embedded PVDF membranes for direct contact membrane distillation and ultrafiltration

Kelvinraj Nursiah, Valentina-Elena Musteata, Sophie Cerneaux, Mihail Barboiu

frontiers | Frontiers in Membrane Science and Technology

TYPE Original Research
PUBLISHED 23 October 2023
DOI 10.3389/frmst.2023.1241526

OPEN ACCESS

EDITED BY
Santanu Karan,
Central Salt and Marine Chemicals Research Institute (CSIR), India

REVIEWED BY
David Martínez Díaz,
Rey Juan Carlos University, Spain
Arcadio Siotto Díaz,
Rey Juan Carlos University, Spain

*CORRESPONDENCE
Sophie Cerneaux,
sophie.cerneaux@umontpellier.fr
Mihail Barboiu,
mihail-dumitru.barboiu@umontpellier.fr

RECEIVED 16 June 2023
ACCEPTED 10 October 2023
PUBLISHED 23 October 2023

CITATION
Nursiah K, Musteata V-E, Cerneaux S and Barboiu M (2023), Artificial water channels-embedded PVDF membranes for direct contact membrane distillation and ultrafiltration.
Front. Membr. Sci. Technol. 2:1241526.
doi: 10.3389/frmst.2023.1241526

Artificial water channels-embedded PVDF membranes for direct contact membrane distillation and ultrafiltration

Kelvinraj Nursiah[1], Valentina-Elena Musteata[2], Sophie Cerneaux[1]* and Mihail Barboiu[1]*

[1]Institute Europeen des Membranes, Adaptive Supramolecular Nanosystems Group, University of Montpellier, Ecole Nationale Supérieure de Chimie de Montpellier-Centre National de la Recherche Scientifique, Montpellier, France, [2]Core Labs, King Abdullah University of Science and Technology (KAUST), Thuwal, Saudi Arabia

Innovative self-supported flat-sheet polyvinylidene fluoride (PVDF) membranes were developed incorporating amphiphilic I-quartet Artificial Water Channels (AWCs) and applied for membrane distillation (MD) and Dyes Ultrafiltration (UF). The presence of AWCs was aimed to increase the amount of water within hydrophobic PVDF pores increasing water permeability and preserving high selectivity and consequently to improve the MD and dyes UF performances. We explored novel strategies in which water channels structures contribute to water cluster stabilization and the increase of water (vapors or liquid) within hydrophobic pore structures. With this novel strategy in mind, three PVDF polymer grades with different molecular weights as well as the variation of their mass concentration as well as of AWCs were studied to shed in light their influence on the water permeability using a dead-end filtration setting. An enhanced water permeability of 75.3 $L.m^{-2}.h^{-1}.bar^{-1}$ was attained for the PVDF-AWC hybrid membrane prepared using 16 wt% PVDF (530,000 g/mol) and 0.05 wt% AWCs when compared with a reference membrane with a water permeability of 30.6 $L.m^{-2}.h^{-1}.bar^{-1}$. The MD performances of both membranes were assessed using a 35 g/L NaCl aqueous solution to yield a salt rejection of 95.3% and 85.2%, respectively. Furthermore, both the reference and the PVDF-AWC membranes showed improved separation performance in terms of rejection efficiency and dye permeability for binary dyes mixture as compared to single dyes. Among all the tested membranes, while methylene blue was completely removed in both cases, the 14 wt% PVDF membrane incorporating 0.075 wt% AWC showed a methyl orange rejection efficiency of up to 99.8% compared to 98.4% for its reference membrane. This hybrid membrane also displayed an almost doubled filtered dye feed permeability of 84 $L.m^{-2}.h^{-1}.bar^{-1}$, compared to 40 $L.m^{-2}.h^{-1}.bar^{-1}$ for its 14 wt% PVDF reference membrane.

KEYWORDS

PVDF, AWC, direct contact membrane distillation, dye rejection, ultrafiltration

1 Introduction

In the field of seawater desalination, energy friendly processes, which are easier to implement need to be considered. Particularly in systems of decentralized fresh water production, one such interesting option is membrane distillation (MD). MD is a process based on a vapor pressure difference, whereby polymeric and ceramic hydrophobic membranes are used. Compared to other membrane separation processes such as nanofiltration (NF) or reverse osmosis (RO), MD possesses some attractive features such as low operating temperatures and low hydrostatic pressure with no need of an applied transmembrane pressure. MD can be considered as a cost effective and competitive process for desalination of brackish water and seawater, that may also be implemented in integrated separation systems in particular with the use of alternative energy sources such as solar energy (Mulder, 1996; Ulbricht, 2006; Pendergast and Hoek, 2011). Two major drawbacks limit the effective use of MD at the industrial scale, namely, the low permeate flux compared to other separation techniques and the pore-wetting phenomena (Chamani et al., 2021). Membrane distillation is a thermally driven separation process whereby the porous hydrophobic membrane separates the saline solution (feed) into a highly concentrated saline solution (brine) and a cold distillate (permeate). The principle of this separation process lies on a temperature difference, allowing only water vapor to pass from the hot feed side, in direct contact with the membrane surface, of higher vapor pressure to the cold distillate of lower vapor pressure. Hence, the properties of the membranes have to be well defined since a hydrophobic porous material will block the passage of liquid by surface tension force while favoring the transfer of vapor (Hsu et al., 2002). Membrane porosity along with pore size are key factors influencing the process as they govern the water flux even though too large pore sizes may favor pore wetting and thus salt permeation through the membrane.

On the other hand, the use of commercial synthetic dyes is widely spread in the chemical industry and represents another challenge towards recovery and reuse of water worldwide. Various industries such as textile, plastics, food and pharmaceuticals, to name a few, consume annually over 7×10^5 t of dyes for their productions (Chen et al., 2015; Lin et al., 2016; Minitha et al., 2017; Sharma et al., 2018). It has been reported that approximately 10%–15% of the dye amount is released into water sources as untreated effluent (Shaban et al., 2017). In addition, the toxicity of these compounds adversely affects the aquatic flora. Dye removal from wastewater prior to discharging into receiving waters is therefore necessary to preserve the aquatic system. To date, a variety of physicochemical and biological technologies have been developed for dye treatment, comprising of membrane filtration, coagulation/flocculation, precipitation, flotation, adsorption, advanced chemical oxidation, and aerobic and anaerobic biological processes (Amini et al., 2011; Nguyen and Juang, 2013; Dasgupta et al., 2015).

Pressure-driven membrane filtration has emerged as a viable solution in this field, owing to the numerous advantages, namely, easy operation, low energy requirement and significant separation efficiency that they offer over other technologies. However, these techniques such as microfiltration (MF) and nanofiltration (NF) still have their limitations. The large pore sizes of MF membranes restrict their use in this field due to their failure to remove dye molecules with molecular weights ranging from a few hundreds to over a thousand Dalton. NF on the other hand provides efficient rejection for most dyes but the large energy requirements associated with this technique renders it complicated at industrial scales. Ultrafiltration (UF), a technique placed between MF and NF, combines the advantages of both to provide satisfactory efficiency with less energy consumption. As such, UF is gaining a lot of attention in the field of dye effluent treatment.

Polytetrafluoroethylene (PTFE), polyethylene (PE), polypropylene (PP) and PVDF are the most commonly used polymers for MD membrane production (Wang and Chung, 2015). Among these hydrophobic materials, PVDF has been attracting much more attraction than its counterparts for this purpose recently. While, PVDF has already been proven to be a material of choice in ultrafiltration and microfiltration for various separation purposes over the years, it is now being considered as potential candidates in MD applications owing to their outstanding properties, such as high hydrophobicity, which implies high LEP, low thermal conductivity, low fouling rate, excellent thermal and chemical stability along with excellent mechanical strength and long term performance. PVDF is one of the most explored polymers for the fabrication of MD membranes because of its excellent morphological properties that lead to the formation of highly porous and permeable films and hollow fibers (Tarvainen et al., 1999). In addition, PVDF exhibits some outstanding properties such as high mechanical strength, thermal stability, chemical resistance and hydrophobicity. The PVDF low surface energy of makes it an attractive material to prepare hydrophobic membranes. Flat-sheet membranes are also characterized by a higher mass transfer coefficient and better antifouling properties compared to other configurations. Over the years, the interesting aforementioned characteristics of PVDF have been further exploited to develop MD membranes presenting enhanced performance. As such, several works have been reported on the fabrication of nanofiber membranes using PVDF as the starting material. Kim et al. (Kim et al., 2023) used PVDF-HFP (PVDF-co-hexafluoropropylene) to prepare crosshatched nanofiber membranes for MD application. Their membranes exhibited an enhanced permeate flux of 65 kg/m^2.h and a salt rejection of 99.99%. Zhou et al. (Zhou et al., 2023) also made use of PVDF-HFP polymer to fabricate a superhydrophobic membrane (surface contact angle: 158°). The reported permeate flux of 33.45 kg/m^2.h and 99% salt rejection of these membranes were higher compared to hydrophobic membranes fabricated with the same material. The blending of PVDF with other materials, such as graphene oxide (GO), for the fabrication of Mixed Matrix Membranes (MMMs) for MD applications has also been attracting a lot of attraction. Hui Ting et al. (Hui Ting et al., 2023) developed a MMM using PVDF and reduced graphene oxide (rGO). The permeate flux of their hybrid membranes showed a 32% enhancement of the permeate flux compared to the reference membranes and a salt rejection of 99.99%. Furthermore, PVDF is widely used for ultrafiltration (UF) membrane fabrication due to its good film-forming ability, thermal stability, and excellent chemical and aging resistance (Srivastava et al., 2011; Kang and Cao, 2014; Nikooe and Saljoughi, 2017). Researches on the use PVDF membranes for dye removal have shown interesting results with pure water permeability values of 1.2–5 $L.m^{-2}.h^{-1}.bar^{-1}$ along with 77%–94% dye retentions (Nikooe and Saljoughi, 2017).

The literature reports five different methods to elaborate polymeric membranes, that are non-solvent induced phase separation (NIPS), vapor-induced phase separation (VIPS), electrospinning, track stretching and sintering. The phase inversion method is widely applied for commercial polymer membranes synthesis due to their simple processing, flexible production scales and low cost (Liu et al., 2011). The four main types of phase inversion methods generally applied for the production of polymer membranes are NIPS, VIPS, thermally-induced phase separation (TIPS) and solvent evaporation-induced phase separation (SEIPS). NIPS, VIPS and TIPS are generally applied for the production of polymer membranes (van de Witte et al., 1996; Kim et al., 2015). NIPS is the main technique used to produce flat sheet PVDF membranes. This method involves a ternary composition usually including a polymer, a solvent and a non-solvent (Wang and Lai, 2013). The first step consists in mixing at least a polymer and a solvent to form an initial homogeneous solution called a dope solution. The prepared solution is then cast as a thin film on a support or extruded through a die to generate the membrane as flat sheets or hollow fibers, respectively (Wang and Lai, 2013). The final step corresponds to the phase separation process in which the material is placed in a coagulation bath containing a non-solvent or a poor solvent for the polymer. The phase separation occurs when the solvent exchanges with the non-solvent and the precipitation of the polymer occurs in the polymer solution. As a result of this fast mechanism, anisotropic porous membranes are obtained. More precisely, the structure of the membranes is asymmetric with a dense skin layer and displaying finger macrovoids throughout the porous cross-section, also identified as the support layer. NIPS can yield asymmetric membranes with different pore sizes for a variety of applications.

The dense skin layer generated in asymmetric membranes during NIPS acts as a barrier for the process. There exists the need to enhance the overall porosity of the membrane. To this end, recently the use of additives in dope solutions has significantly developed. Studies have investigated the influence of additives on pore formation and pore interconnectivity in membrane morphology (Guillen et al., 2011). Several works have reported the preparation of polymer membranes incorporating different additives or hydrophilic polymers such as polyvinyl-pyrrolidone (PVP), polyethylene-glycol (PEG) (Guillen et al., 2011). Their results show an improvement of membrane gravimetric porosity and permeability leading to better MD performances. The incorporation of the inorganic LiCl salt proved to have a drastic influence on the asymmetric PVDF membrane structure with an upper layer with large macrovoids for MD application (Tomaszewska, 1996). The introduction of hydrophilic polymers and other additives such as inorganic salts has gained some ground in membrane preparation, more and more studies are focusing on the incorporation of other types of additives for the development of novel polymer membranes with improved performance. Among those additives, namely, carbon nanotubes (Kumar et al., 2019), silica nanoparticles (Aquino et al., 2018; Julian et al., 2019) and amphiphilic copolymers (Zhao et al., 2013) can be cited. Those novel membranes have shown to have enhanced properties such as higher fouling-resistance (Yi et al., 2012). The use of additives is therefore now wide spread in the fabrication of polymer membranes, such that their intrinsic properties can be tuned to have the desired effect during the various applications they are designed for.

The focus of the present work was to develop mechanically resistant polyvinylidene fluoride (PVDF) self-supported flat-sheet hydrophobic membranes with enhanced water permeability and high salt rejection using the NIPS method. For this purpose, Artificial Water I-quartet Channels (AWCs), self-assembled from amphiphilic hexylureido-ethyl-imidazole (HC6) monomers were incorporated within the polymeric PVDF matrix (Di Vincenzo et al., 2021). Artificial Water Channels are synthetic mimics of biological water channel aquaporins, which allow them the possibility of combining high water permeability with high water/solute selectivity along with higher processability and stability compared to protein channels (Di Vincenzo et al., 2021). The presence of AWCs within the hydrophobic polymer matrix is thus expected to create selective hydrophilic water H-bonding regions on the surface of hydrophobic pores avoiding water condensation and enhancing water absorption within pores present as vapors under nanoconfined conditions (Di Vincenzo et al., 2021). We postulate that an optimal amount of channels can flow freely water under the PVDF hydrophobic pores, accelerating thereby the permeate flux without altering the selectivity. The NIPS method was used for the preparation of the AWC embedded PVDF membranes to obtain porous membranes with enhanced porosity and consequently higher flux during MD process. The reference PVDF membranes and their corresponding AWC(HC6)-modified membranes were synthetized and selected based on the above-discussed properties. The strategy developed was to evaluate firstly the influence of three PVDF having different molecular weights, namely, 180,000, 275,000 and 530,000 g/mol and secondly, the influence of the PVDF content (16–20 wt%) on the membrane structures and performances. The performances of the newly developed PVDF-AWC reference and hybrid polymer membranes were then evaluated in Direct Contact Membrane Distillation of a 35 g/L NaCl solution and investigated towards the separation of single dyes, the anionic Methyl Orange (MO) and the cationic Methylene Blue (MB) along with their binary dyes mixture.

2 Material and methods

2.1 Materials

The PVDF pellets with various grades of 180,000, 275,000 and 530,000 g/mol and the N,N-Dimethylacetamide (DMAc) used as solvent were purchased from Sigma-Aldrich France. The sodium chloride salt (≥99.0%) and the Methyl Orange (MO), Methylene Blue (MB) and Eriochrome Black T (EBT) dyes were all supplied from Sigma-Aldrich, France. Milli-Q water (18 MΩ cm) was used as non-solvent for the membrane preparation and in the Direct Contact Membrane Distillation (DCMD) experiments. The HC6 AWCs were synthesized following a procedure described elsewhere (Le Duc et al., 2011).

2.2 Reference and PVDF-AWC membranes preparation

The PVDF-AWC hybrid membranes were synthesized using the NIPS technique. Polymer dope solutions were prepared by

TABLE 1 Average atomic percentage of C, N, O and F present in PVDF-AWC M1-a membrane obtained by EDX spectroscopy.

C (%)	N (%)	O (%)	F (%)
64.50	14.37	17.20	3.24

TABLE 2 Phase transitions observed in the different samples.

	Phase transitions (°C)
PVDF	66.95, 165.79
HC6	127.59
MEMBRANE M0-A	64.88, 104.36, 158.06
MEMBRANE M1-A	87.97, 116,47, 156.26

dissolving the PVDF pellets of different molecular weights and the HC6 molecules in DMAc at 55°C for 6 h. After a degassing period of 18 h at 25°C, the dope solutions were cast using a K Control Coater (Ericksen France) equipped with a casting knife (K202 Micrometer Adjust Applicator 200 mm, Ericksen France) adjusted at a gap of 250 µm on a glass plate. After being exposed to air for 15 s, the nascent membranes were immersed in a non-solvent ultrapure water bath (18 MΩ.cm) at 25°C for 5 min. The obtained flat-sheet membranes were rinsed with running ultrapure water to remove both the residual solvent and non-solvent. Finally, the membranes were stored in a water bath at room temperature until further use. The various dope solution compositions used to prepare the membranes to be tested in DCMD experiments are reported in Supplementary Tables S1, S2 for the ones dedicated to the dye separation experiments.

Keeping constant the amount of PVDF (530,000 g/mol) at either 16 (a), 18 (b) or 20 (c) wt%, the DMAc quantity was adjusted from 84 wt%, 82 wt% and 80 wt%, respectively to insert 0.05 wt% of HC6 (series of M1 membranes), 0.075 wt% of HC6 (series of M2 membranes) and 0.1 wt% of HC6 (series of M3 membranes) as displayed in Table 1. In brief, the membrane code can be understood as such: the number reports to the HC6 wt% concentration and the letter represents the PVDF wt% concentration. M0, M1, M2 and M3 membranes correspond to 0; 0.05; 0.075 and 0.10 wt% HC6 respectively and a, b and c correspond to 16; 18 and 20 wt% PVDF respectively. As an example, the reference membrane (without HC6) prepared with 16 wt% of PVDF and 84 wt % of DMAc is noted M0-a. The one containing 18 wt% of PVDF and 82 wt% of DMAc is noted M0-b and finally the M0-c membrane is composed of 18 wt% of PVDF and 80 wt% of DMAc.

Regarding the various PVDF-AWC hybrid membranes prepared in view of dye separation experiments, we varied the PVDF, HC6 and DMAc concentrations in the dope solutions as shown in Table 2. Maintaining the amount of PVDF at either 14 (1, 1a-c), 16 (2, 2a-c), 18 (3, 3a-c) or 20 wt% (4, 4a-c), the DMAc quantity was adjusted from 86 wt%, 84 wt%, 82 wt% and 80 wt%, respectively to insert 0.025, 0.05 and 0.075 wt% of HC6. In the membrane code of Table 2, MR stands for Membrane Reference and MH for Membrane containing HC6. MO and MB represent the single dyes whereas MOB and MOEB stand for the dyes mixtures of MO-MB and MO-EBT, respectively.

2.3 Membranes characterization

2.3.1 Morphological and structural analyses of the hybrid membranes

The top surface and cross-section morphological structures of the membranes were observed using a scanning electron microscopy (SEM). The images were acquired on a Magellan SEM (ThermoFisher Scientific) in high resolution immersion mode, using 5 kV acceleration voltage, a beam current of 50 pA and 4 mm working distance. For cross-sectional imaging the membranes were cryogenically fractured in liquid nitrogen. The samples were mounted with carbon tape on aluminum stub and sputter-coated with 4 nm iridium before imaging. An Oxford X-MaxN EDX detector for Energy-Dispersive X-Ray spectroscopy allowed the determination of the average atom percentage of carbon, oxygen and nitrogen present in the HC6 modified membranes.

Scanning transmission electron microscopy—energy dispersive x-ray spectroscopy (STEM-EDX) maps were acquired on a Titan Themis TEM (ThermoFisher Scientific) equipped with a Four-Quadrant SuperX EDS detector.

X-Ray powder diffraction (XRD) was performed on hybrid membranes samples to attest the presence of HC6 entities within their polymer matrices. We know from previous studies, that the XRD powder diffraction pattern of self-assembled I quartet AWCs correspond to a lamellar crystalline phase self-organization (Le Duc et al., 2011).

2.3.2 FTIR spectroscopy

Attenuated Total Reflectance-Fourier Transform Infrared spectroscopy (ATR-FTIR) was used to analyze the chemical structure of the powdered membranes. ATR-FTIR spectra were recorded on a NEXUS spectrometer in the region of 650—4,000 cm^{-1}. A dope solution of the virgin membrane with a 9:1 polymer to solvent ratio was prepared while for the HC6 modified membranes (M1, M2 and M3 series of Table 1) the ratio was 9:1.58:8.42 for solvent, PVDF and HC6, respectively. Droplets of the dope solutions were subjected to evaporation in a Petri dish such that nanocrystals were obtained.

2.3.3 Thermal analyses

The pulverized membranes were also analyzed by Thermogravimetry (TGA) and Differential Scanning Calorimetry (DSC) to evidence their behavior when exposed to an increased temperature. The weight loss determined by TGA provided useful information related to the thermal decomposition of both polymer and HC6 moieties. The DSC measurements indicated physical phase transitions occurring within the prepared membranes upon temperature increase.

2.3.4 Membranes Liquid Entry Pressure of water (LEP_W) and pure water permeability (PWP) measurements

To evaluate both the hydrophobicity and porosity of membranes, the Liquid Entry Pressure of water (LEP_W) is sought. This parameter is a significant membrane characteristic that is defined as the minimum transmembrane pressure required for the feed solution to penetrate the pore size; in other terms it corresponds to the pressure at which the first drop of water will permeate through the membrane.

The Cantor-Laplace Eq. 1 (Pal, 2015) correlates the maximum pore size r_{max} to the degree of hydrophobicity of the membrane identified by the water contact angle σ:

$$LEP_W = \left(-2\gamma_L \cos\sigma\right) \div r_{max} \quad (1)$$

where Υ_L represents the surface tension of the tested liquid.

The LEP_W is directly proportional to the water contact angle and inversely proportional to the membrane pore size. A high LEP_W would imply a hydrophobic material having small pore sizes and a low porosity. This would result in a low water permeability and hence a low water flux as a high porosity and large pore sizes are generally associated to a higher water flux (Tan and Rodrigue, 2019).

In this study, the LEP_W of the prepared membranes was determined along with the pure water permeability to characterize their wetting resistance. For this purpose, a dead-end filtration set-up (Sterlitech cell) filled with ultrapure water was used. The membrane was placed inside the cell and nitrogen pressure applied on the feed side was increased step-wise after a few minutes of stabilization time respected after each increment (0.69 bar). The membrane was first compacted at a pressure of 2 bar higher than the LEP_W during 20 min. Going backwards from the compaction pressure to the LEP_W, water flux was recorded and plotted as a function of the transmembrane pressure to determine the PWP of the membrane was determined by considering the gradient of the slope of the obtained linear graph.

2.3.5 Water contact angle measurements

The hydrophobicity of the membranes was estimated by measuring the water contact angle of a water droplet of 5 µL deposited on the membrane surface. The contact angles were measured by a lab-made contact angle goniometer equipped with a camera. As soon as the water droplet was deposited on the membrane surface, a picture was instantly captured. The reported values are the average of three measurements at different zones on the membrane surface.

2.3.6 Membranes porosity determination

The membrane porosity ε was determined by the gravimetric method, which consists in finding the weight of liquid contained in the membrane pores. Membranes were cut into 1 × 1 cm pieces and immersed in ethanol for 30 min. After mopping with tissue paper, the wet membranes were weighed and the porosity ε was calculated according to Eq. 2 (Roshani et al., 2018)

$$\varepsilon = \left[(m_2 - m_1)\rho_1\right] \div \left[\rho_1 m_2 + (\rho_2 - \rho_1)m_1\right] \quad (2)$$

where m_1 is the dry weight and m_2 represents the wet weight of the membranes. ρ_1 and ρ_2 are the densities of PVDF (1.78 $g.cm^{-3}$) and ethanol (0.79 $g.cm^{-3}$), respectively. The porosity of the membrane was defined as the volume of the pores divided by the total volume of the membrane.

2.4 Membranes performances in direct contact membrane distillation (DCMD)

A laboratory-scale MD pilot was used for DCMD experiments. The self-supported flat-sheet membranes were tightly clamped between two Teflon plates leaving an effective operation area of 2.86 × 10^{-3} m^2. An aqueous sodium chloride solution (35 g/L) composed the feed side and the permeate was directly recovered in the circulating cooling system (18 MΩ cm water). The feed inlet temperature T_f was fixed at 70°C (±2°C) and the distillate inlet temperature T_p was maintained at 20°C (±1°C). Two independent peristaltic pumps were used to circulate the feed solution and the cold permeate one. The pump for the latter helped maintaining a flow rate of 150 mL/min. The main operating conditions used in the DCMD experiments are reported in Supplementary Table S3.

Throughout the DCMD process, the distilled permeate was diluted in the cold circulating water. The diluted solution was collected, weighed and transferred back in the cold circulation loop every 30 min. The salt concentration *Cp* collected in the distilled permeate was monitored by conductivity σ ($S.m^{-1}$) with a VWR ® Phenomenal ® MU 6100H conductometer and calculated according to a calibration curve ($Cp = \sigma/5.5758$). Finally, the water permeate flux was calculated according to Eq. 3.

$$J_w = \Delta m / A.t \quad (3)$$

where J_w represents the water permeate flux (kg/m^2. h), Δm is the permeate weight (kg), A is the effective membrane surface area (m^2) and t is the experiment time duration (h).

The salt rejection R was determined according to Eq. 4.

$$R\,[\%] = \left(1 - \left(C_p \div C_f\right)\right) \times 100 \quad (4)$$

where C_p and C_f represent the NaCl concentration in the distilled permeate and the feed, respectively.

2.5 Membranes performances in dyes separation

A 500 mL stock solution of either Methyl Orange (MO), Methylene Blue (MB) or Eriochrome Black T (EBT) dye at a concentration of 20 mg/L in Milli-Q water (18 MΩ.cm) was prepared to perform the filtration experiments using a Sterlitech cell in a dead-end configuration. The binary dyes mixtures (MO-MB and MO-EBT) were prepared at a total concentration of 20 mg/L in a 1:1 ratio. The feed volume of 300 mL was in contact with the membrane placed at the bottom of the cell giving an effective filtration area of 9.07 cm^2. The experiments were carried out at transmembrane pressures ranging from the determined LEP_W of the membrane to 3 bar at 20°C ± 2°C. For each membrane, the permeability *P* ($L.m^{-2}.h^{-1}.bar^{-1}$) (Eq. 5) of both pure water and dyes mixture solution and the dye retention rate R (Eq. 4) were recorded at the different applied transmembrane pressures.

$$P = V / (A \times t \times \Delta P) \quad (5)$$

where *V* (L) is the volume of permeate flowing across the membrane of an effective area *A* (m^2) in the time period *t* (h) and at the operating transmembrane pressure ΔP (bar).

The dye concentrations in both the feed and the permeate solutions were monitored at 463.5, 660.5, and 529.5 nm for MO, MB and EBT, respectively using the UV-Vis spectrometry and using a Lambert's -Beer calibration curve established for each single dye (MO, MB and EBT) No spectral overlap was expected between the two single dyes for each binary mixture and their mixtures.

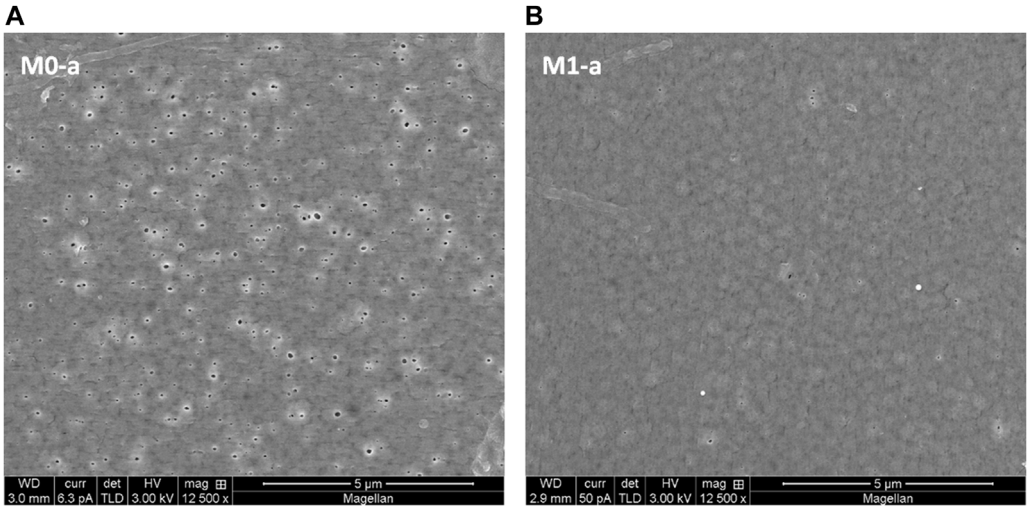

FIGURE 1
SEM micrographs of top surface of 16 wt% PVDF M0-a reference **(A)** and 0.05wt% HC6 modified PVDF-AWC M1-a **(B)** membranes.

3 Results and discussion

3.1 Influence of the PVDF molecular weight and concentration of the AWC concentration on the membranes morphology and chemical structure

While for MD application, studies have shown that the structural morphology of symmetric membranes are better suited, morphology control of asymmetric membranes obtained via the NIPS method remains a viable alternative. The mass transfer mechanism occurring during the phase separation process dictates the final membrane morphology. The shift in structure morphology from asymmetric porous membranes with finger pore-like macrovoids observed in NIPS method to an isotropic sponge-like cross-section morphology with a more open porous surface can be explained by the rate of polymer precipitation, occurring during the phase separation process. A low precipitation rate also referred to as delayed demixing will tend to yield symmetric membranes. A higher precipitation rate, commonly called instantaneous demixing will produce asymmetric membranes (Tan and Rodrigue, 2019).

The hexylureido-ethyl-imidazole HC6 molecule consists of a amphiphilic molecule with a hydrophilic imidazole head, while the hexyl chain makes up for its hydrophobic character. The hydrophobic tail of the HC6 will tend to be more embedded within PVDF at the surface of the membrane. The hydrophilic head will be oriented towards the hydrophilic outside. One would therefore expect for the hydrophobic tail to blend with the polymer matrix and for the hydrophilic head to self-organize via urea H-bonds at the water/DMAc interfaces with a final pending distribution at the membrane surface that remain mostly hydrophobic but decorated with water binding imidazoles that selectively stabilize the vapors of water. This will give rise to micelles or aggregates dispersed throughout the polymeric matrix. We suggest this mechanism to be in line with our hybrid model. The self-assembled arrangement of the clusters in the matrix coupled with the MD performance provides evidence of this mechanism. It should also be noted that, depending on the size of the aggregates, bigger agglomerates incorporating the smaller aggregates might be formed.

SEM micrographs provided useful insights on the morphology of the prepared membranes and allowed for a first approximation of the pore sizes and distribution on the surface. The morphology of the top (Figure 1) and bottom surface (Figure 2) and cross-section (Figure 3) of the M0-a membrane prepared with the 530,000 g/mol PVDF at 16 wt% and M1-a, its corresponding hybrid membrane containing 0.05 wt% of HC6 were compared in. Both membranes present an asymmetric structure with a low porous skin layer on the top surface, This configuration would ensure an efficient PVDF surface modification, allowing for the synergetic selectivity and flux productivity enhancement. However, a careful investigation of the HC6 modified membrane morphology indicates a whole different mechanism. Indeed, while it was expected for the overall porosity to be enhanced by the incorporation of the AWCs, the dense skin layer generally yielded during NIPS process was not exactly as such impacted in our case study (Figure 1).

Indeed, the morphological change was more obvious on the bottom surface), that is the layer in contact with the glass plate support, where nanopores/micropores can be detected on reference and functionalized membrane (Figure 2).

An important shift in structural morphology of the microporous layer adjacent to the macropores and to the bottom surface of the membranes as illustrated by the SEM micrographs presented in Figure 3. Three distinct layers are noted, namely, the film surface, the sublayers adjacent to the surface and deep sublayers (Machado et al., 1999). While we will not elaborate here the thermodynamic approach depicted by ternary phase diagram, which is generally used to model and predict the phase inversion process, attention is brought to the qualitative model proposed by Machado et al. (Machado et al., 1999), in an attempt to highlight the more likely abundance of porous morphologies induced by the presence of the HC6 molecules at the bottom of membrane compared to the reference PVDF membrane. What should be retained from this proposed model, is that the liquid-liquid demixing

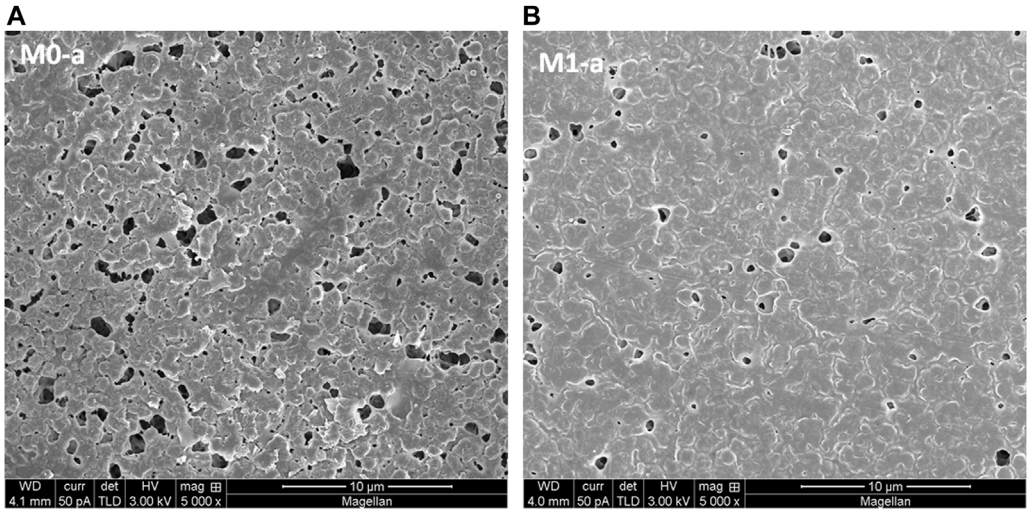

FIGURE 2
SEM micrographs of bottom surface of 16 wt% PVDF M0-a reference **(A)** and 0.05wt% HC6 modified PVDF-AWC M1-a **(B)** membranes.

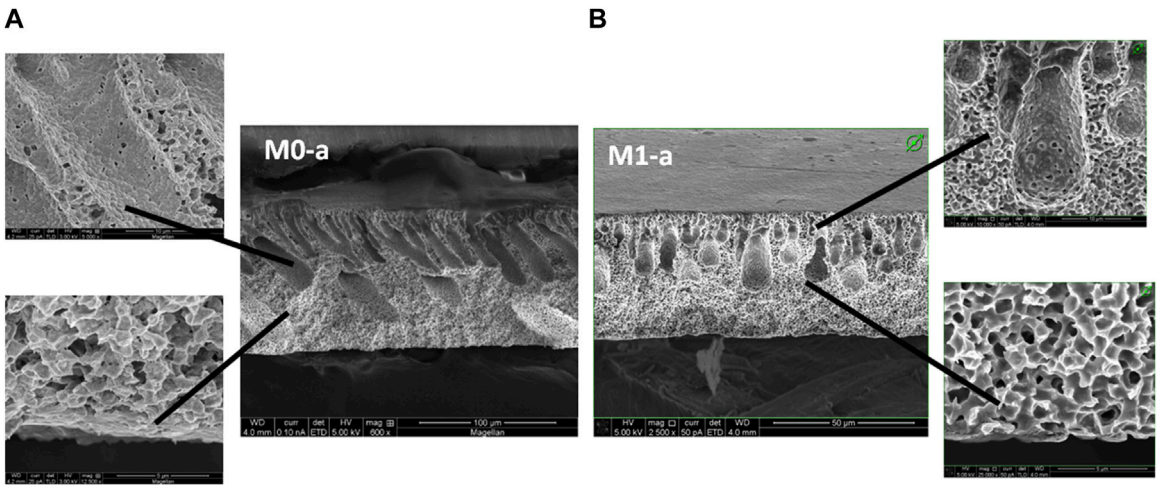

FIGURE 3
SEM micrographs of cross section of 16 wt% PVDF M0-a reference **(A)** and 0.05wt% HC6 modified PVDF-AWC M1-a **(B)** membranes.

dominates membrane formation during the immersion process which can occur at the bottom surface by nucleation and growth, whereby crystallization of polymer globules is mostly favored.

We suggest a possible faster polymer precipitation rate in the case of the HC6-modified membrane during the phase inversion process, with the mass transfer exchange rate between the solvent (DMAc) and the non-solvent (water) occurring at the top surface (film surface) when the glass plate is immersed in the non-solvent bath, also, quite high. This rapid exchange of solvent and non-solvent accounts for the solidification of the polymer rich phase at the film surface, leading to the dense skin layer observed in the modified membrane. It is hypothesized that during this solidification process, the HC6 amphiphilic molecules get embedded in the hydrophobic tails in the PVDF matrix and imidazole hydrophilic groups pending in water. Once the dense skin layer is formed, the diffusion mechanism extends throughout, thus forming the sublayer adjacent to the surface. The diffusion rate being much slower than the liquid-liquid demixing process at the top surface, the HC6 molecules are given more time to self-assemble at the surface of particles and get dispersed throughout the cross-section. As mentioned, at the bottom surface, crystallization of polymer globules decorated with hydrophilic imidazoles will occur. The latter get coated by the HC6, leading to the more noticeable open interconnected porous network due to improved water swelling during the membrane formation.

In contrast, the pristine (reference) membrane presented a less porous structure of inner microporous layer (Figure 3). While the globules are more agglomerated in the reference membrane, the

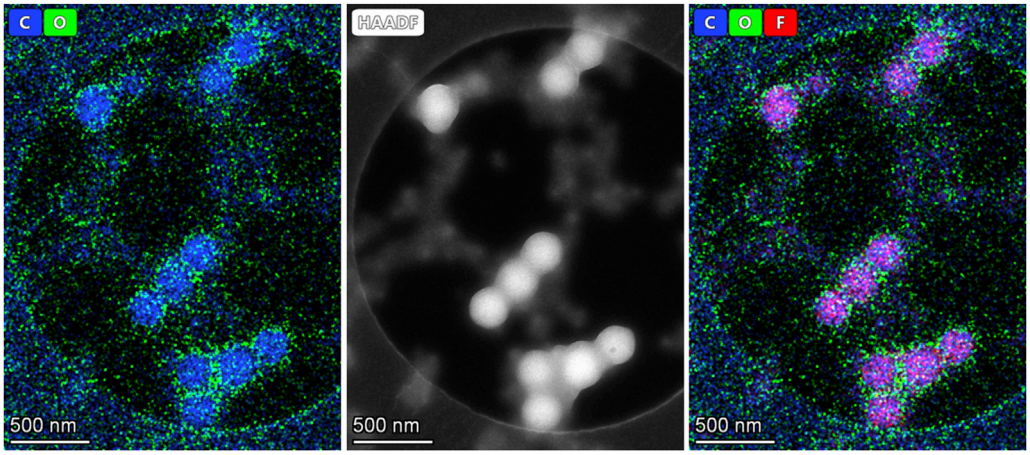

FIGURE 4
Scanning transmission electron microscopy—energy dispersive x-ray spectroscopy (STEM-EDX) maps were acquired on PVDF-HC6 nanoparticles: C (blue) F (red) O (green) the combination of blue and red led to a pink combined color (right image).

presence of more pores are visible in the HC6-modified membrane, with hydration inducing spacing between the globules bearing hydrophilic imidazole groups at the surface. A closer look at the cross-section of the HC6-modified membrane reveals deeper macrovoids, surrounded by a more cellular structure surface of the HC6-modified membrane, M1-a (Figure 3). Pure water permeability (PWP) tests carried out on the two opposite sides (top and bottom surfaces) of the PVDF-AWC membrane provides further evidence of the increased probability of finding the HC6 on the bottom side. The enhanced PWP for the HC6-modified membranes as compared to the pristine membranes are reported for the bottom surfaces.

Indeed, the HC6-modified membrane exhibits a cross section with more pores, cavities or macrovoids as compared to the reference membrane (Figure 3). This observation supports the suggestion that the HC6 particles form aggregates within the polymer matrix, leading to a more hydrated water swelled microstructures, this latter being responsible for the permeation properties (Chuang et al., 2000).

Indeed, the HC6 modified membrane exhibits a cross section with more pores, cavities or macrovoids as compared to the reference membrane (Figure 3), leading to a more symmetric structure. This observation supports the suggestion that the HC6 particles form aggregates within the polymer matrix, leading to a more hydrated water swelled microstructures this latter being responsible for the permeation properties (Chuang et al., 2000).

As described previously, from the SEM micrographs of Figure 2, one can clearly observe the interconnected porous network formed from the crystallization of the polymer globule, coated by the HC6. This hypothesis was confirmed by EDX spectroscopy, providing further evidence of the successful incorporation of the HC6 entities within the PVDF matrix. Indeed, from the data collected in Table 1, one can determine the following formula $C_{12}O_{3.2}N_{2.7}$ that is not so far from the pure HC6 molecular formula $C_{12}H_{22}ON_4$. To observe if there is a preferential assembly of the PVDF HC6 blends in solution and to mimic the phase inversion in water the following experiment was performed. A diluted solution in DMAC with 1% wt. total concentration of PVDF and HC6 (the relative ratio of PVDF was 5: 95 wt%) was prepared and stirred for 1 day. Nanoprecipitation of this solution was done by adding dropwise 0.1 mL of this solution to 1 mL water under magnetic stirring. Samples were prepared by placing a drop of the precipitated solution onto Quatifoil copper grid, blotted with filter paper and let dry for several hours. Scanning transmission electron microscopy—energy dispersive x-ray spectroscopy (STEM-EDX) maps acquired on resulted nanoparticles of 200 nm in diameter are reminiscent with the formation of PVDF cores concentrating C and F elements in the center of particles, while O element provided from HC6 and water molecules are present at the surface and between the nanoparticles (Figure 4). In a such way interparticle nanometric water channels are forming within membrane structure.

The gravimetric method allowed for an estimation of the membrane porosity. Only a slight increase of 9% in porosity was observed for the 0.05 wt% HC6-modified membrane (M1-a). This may be attributed to the thermodynamic instability caused by the incorporation of the AWCs in the polymeric matrix. The amphiphilic character of the HC6 delays the exchange between the solvent (DMAc) and the non-solvent (Milli-Q water), promoting the formation of a porous structure (Khayet et al., 2010; Cui et al., 2014; Fadhil et al., 2016).

To further evidence the presence of the HC6 molecules within the polymer, XRD patterns were recorded on powdered membranes, namely, pure PVDF of 530,000 g/mol molecular weight, HC6 pure compound as powder and nanocrystals, M0-a and M1-a membranes as shown in Figure 5. The (*100*) and (*200*) crystallographic planes are reminiscent of the lamellar crystalline phase of the I-quartet channels composed of HC6. This peak is also present on the pattern of the HC6 nanocrystals obtained from recrystallization in anhydrous DMAc. Compared to the pattern of PVDF powder and PVDF membrane M0-a, the M1-a membrane consisting of PVDF and 0.05 wt% of HC6 is the only one presenting this (*100*) characteristic plane attesting the presence of a lamellar phase in the HC6-modified membrane. The appearance of multiple phases is noted at $2\theta = 10^{\circ}$ corresponding to the reticular plane (200). This

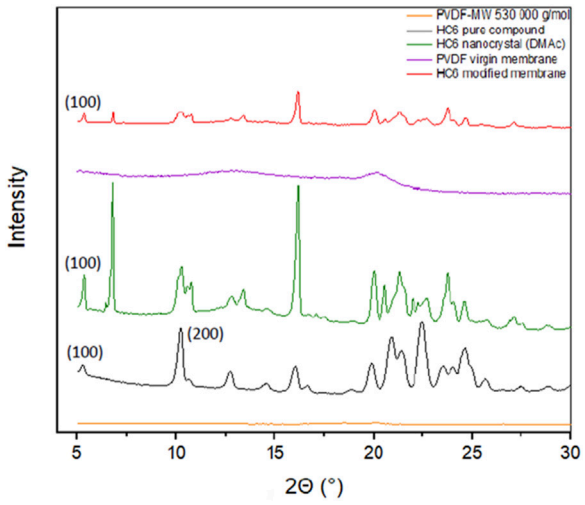

FIGURE 5
Powder X-ray diffraction patterns of (orange) PVDF-MW 530,000 g/mol grounded pellets (black) pure HC6 compound (green) nanocrystal HC6 I-quartet AWC crystallized in anhydrous DMAc, purple (PVDF M0-a reference membrane) and (red) M1-a HC6-modified membrane.

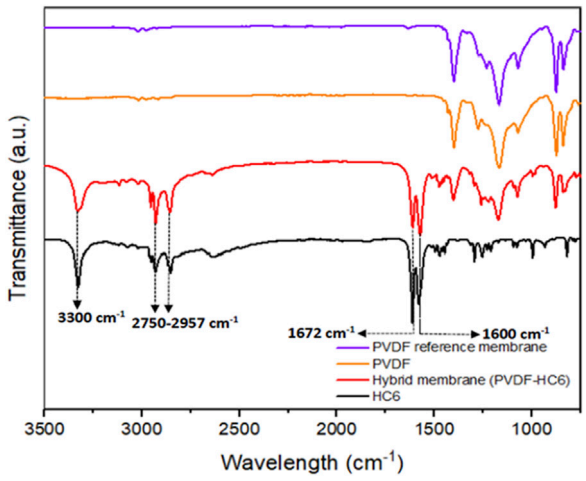

FIGURE 6
FTIR-ATR spectra for (purple) PVDF reference membrane (orange) PVDF pellet-MW 530,000 g/mol (red) HC6-modified membrane and (black) pure HC6 compound.

similar formation in the HC6 nanocrystal in DMAc and is the HC6-modified M1-a membrane are significantly similar.

Another interesting way to verify the presence of the HC6 AWCs within the polymer matrix is to study the different samples by FTIR-ATR. The FTIR spectra of the PVDF pellets, the PVDF reference membrane M0-a, the hybrid PVDF-HC6 membrane M1-a and the pure HC6 compound were thus analyzed (Figure 6).

The sharp band centered at around 3,300 cm^{-1} is related to the O-H stretching vibration of strongly H-bonded water molecules within I-quartet channels composed of HC6. The presence of less bounded water molecules within the matrix accounts for the broadening of this band in the PVDF-HC6 hybrid membrane. The $CH_{asymmetric}$ and $CH_{symmetric}$ stretching vibration bands are characteristic of the alkyl chains in the range 2,750—2,957 cm^{-1}. In addition, the bands at 1,600 and 1,672 cm^{-1} are characteristic of urea C=O bonds for both, the HC6 compound and the HC6-modified membranes, but with different intensities, suggesting the incorporation of the HC6 artificial water channels. The FTIR data confirmed that HC6 compound was successfully incorporated within the matrix of the HC6-modified membrane.

TGA and DSC analyses were performed on powders of the prepared membranes samples to evaluate their thermal properties. Two weight losses are found from 400°C to 500°C (57.5%) and up to 1,000°C (41.6%) leading to the almost total decomposition of the pellets. The water loss starts at lower temperature of 100°C while the degradation of the HC6 molecules yield to a weight loss of 91% at 450°C. At 650°C, the HC6 is totally decomposed. When looking at the reference M0-a membrane, three weight losses of 4% up to 150°C, 63% up to 450°C and a last one of 33% up to 600°C appeared. They may correspond to water and/or solvent evaporation in a first stage that was not present for the PVDF pellets and to the progressive decomposition of the polymer matrix upon temperature as previously observed. The thermogram of the HC6-modified membrane M1-a is characterized by more peaks of decomposition that proves the incorporation of the HC6 molecules within the matrix. The first water loss is encountered before 100°C (2.4%), two others appear between 100°C and 350°C (56.1%) and the last ones up to 650°C (41.1%). To try to better understand how the HC6 is embedded in the PVDF matrix, we did the DSC analyses of the M0-a and M1-a membranes as reported in Table 2. The PVDF glass transition temperature is almost constant at about 67°C and 65°C in the PVDF pellets and M0-a membrane, respectively. The same behavior is noticed for the second DSC peak at 165.8°C in PVDF alone compared to 158.1°C in M0-a. However, a shift to a higher temperature of 88°C is observed for the PVDF-HC6 M1-a membrane with. Concerning the HC6 molecules, the lone phase transition visible is at 127.6°C, peak that is not present in the DSC curve of the M0-a membrane and shifted in the M1-a membrane at a lower temperature of 116.5°C. The different phase transitions observed for the PVDF membrane M1-a indicate the formation of a hybrid portion at the surface of the HC6-modified membrane.

3.2 Effect of the concentration of PVDF (530,000 g/mol) on the LEP_W and pure water permeability

The reference and hybrid membranes with a PVDF (530,000 g/mol) concentration fixed at 16, 18 and 20 wt% were prepared to evidence their performance in filtration in terms of both the LEP_W and pure water permeability (Figure 7; 8).

It appears that the LEP_W of the M0-a is similar at 16 and 18 wt% of PVDF content (0.69) compared to the 20 wt% (1.38). Regarding the M1-a membrane, a similar LEP_W value of 0.69 is obtained at 18 and 20 wt% of PVDF compared to 0.23 for the membrane prepared with 16 wt% of PVDF. Membrane M2-a

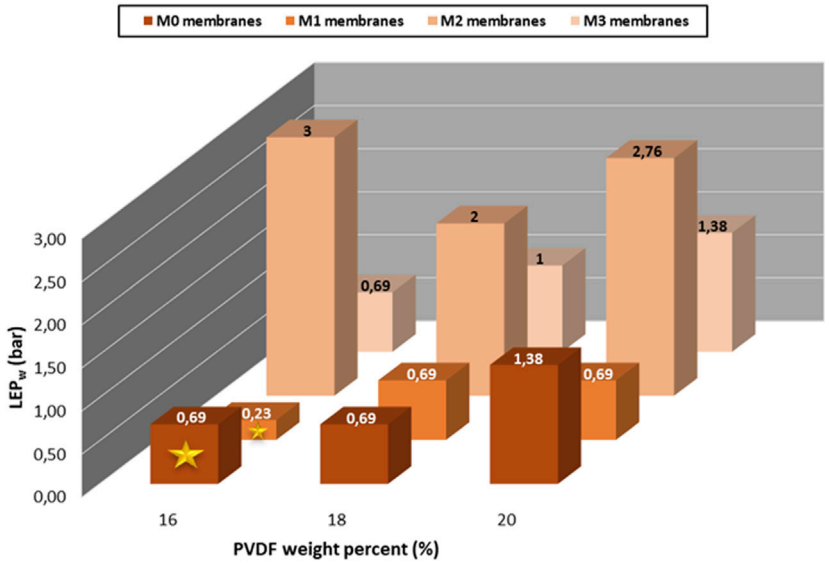

FIGURE 7
LEPW of the HC6-modified membranes prepared from PVDF-MW 530,000 g/mol as a function of the PVDF concentration.

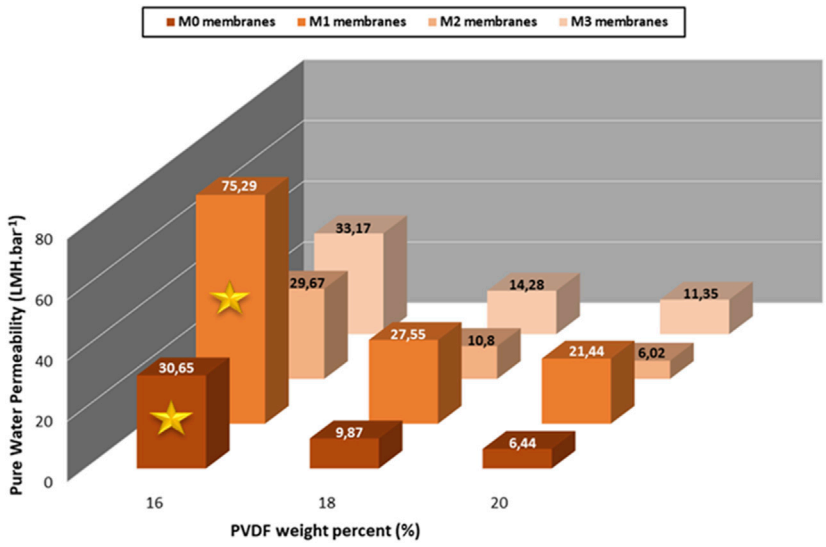

FIGURE 8
PWP of HC6-modified membranes prepared from PVDF-MW 530,000 g/mol as a function of the PVDF concentration.

containing 0.075 wt% of HC6 shows the highest LEP_W values whatever the concentration of PVDF. When increasing the HC6 content to 0.1 wt% in M3-a, the behavior seems to be similar as the M0-a reference membrane except at 18 wt% of PVDF.

From these results, it seems that the membranes with higher loading of HC6 are more permeable than the reference M0-a and M1-a. This can be attributed to the hydrophilic AWC layer formed by bearing HC6 molecules at the surface of the nanoparticles. In addition, a high concentration of polymer is expected to lead to a low porosity of the membranes affecting thus the water flux, whereas a lower porosity may result in a lower water permeability. As evidenced in Figure 8, the highest water permeability of 75.3 $L.m^{-2}.h^{-1}.bar^{-1}$ was obtained for the HC6-modifed membrane M1-a prepared with 16 wt% of PVDF, followed by the M0-a reference membrane with a permeability of 30.6 $L.m^{-2}.h^{-1}.bar^{-1}$. We also noticed that higher content of PVDF (18 and 20 wt%) in all membranes yielded to low PWP. Therefore, the content of 16 wt% appeared to be the optimum value for the PVDF content.

TABLE 3 Desired membrane parameters for MD reported in the literature.

Parameters	Range	Ref
Contact angle (°)	80–160	El-Bourawi et al. (2006), Pramanik et al. (2016)
Pore size (μm)	0.01–0.5	Darvishmanesh et al. (2011), Adnan et al. (2012), Akbari et al. (2012)
Porosity (%)	35–93	Adnan et al. (2012), Drioli et al. (2015), Lu et al. (2017)
LEP_W (bar)	0.4–0.7	Hamzah and Leo (2016)
Thermal conductivity (W/m K)	0.11–0.27	Ahmad et al. (2015), Tai et al. (2023)

TABLE 4 LEP_W, contact angle (CA), pore size distribution and porosity of M0-a and M1-a membranes.

Membrane code	LEP_W (bar)	Ca (°)	Maximum pore size (μm)	Minimum pore size (μm)	Porosity (%)
M0-a	0.7 ± 0.1	107 ± 1	1.44	0.28	24
M1-a	0.2 ± 0.1	111 ± 1	4.48	0.52	33

Water contact angle measurements were also carried out on the different sets of membranes to analyze their hydrophobicity degree and try to correlate the values with the LEP_W results. The reference membrane M0-a had an average contact angle of 107° ± 1° while the HC6-modified membrane M1-a displayed a slightly higher contact angle of 111° ± 1°. M2-a and M3-a with a higher HC6 loading are characterized by contact angles of 104° ± 1° and 89° ± 1°, respectively. The low water contact angle recorded for membrane M3-a could not be further assessed. Indeed, the Cantor Laplace equation is not applicable for angles below 90° (Chang et al., 2021).

Therefore, the presence of hydrophilic HC6 molecules has a slight impact on the contact angle and obviously on the membrane surface morphology and porous structure.

Among the collected data, two stand out membranes could be singled out, notably the reference M0-a membrane and its corresponding HC6-modified membrane M1-a. We will thus focus on these two membranes for the rest of the study.

The higher water permeability demonstrated by the hybrid membrane M1-a as compared to its reference membrane M0-a can be justified by its lower LEP_W value being 0.2 bar against 0.7 bar for M0-a, which would mean that the former would present a higher maximum pore size as per the Cantor Laplace Equation 1. The higher maximum pore size of the HC6-modified membrane (4.48 μm) as compared to that of the reference PVDF membrane (1.44 μm) provides evidence for the higher water permeability of the former.

To further demonstrate the efficiency of the AWCs with the PVDF matrix, we did some water vapor transport experiments using a gas separation pilot. The PVDF reference membrane M0-c showed a flux of water vapors of 109 $g.m^2\ j^{-1}$ and the PVDF-AWC hybrid one M4-c a flux of water vapors of 161 $g.m^2\ j^{-1}$ when tested at a temperature around 25°C–30°C. A hybrid membrane with the highest wt% concentration of PVDF used in the present work, namely, 20 wt%, and a higher loaded concentration of HC6 (1 wt%) were prepared for the water vapor transport experiments. A higher wt% concentration of HC6 than that used in the DMAC experiments (0.1 wt%) was chosen so as to evidence their effective presence within the membrane's matrix. From the data obtained, it is obvious that the presence of the AWCs within the polymer network has for effect to facilitate the transport of the water vapor since a 60% increase of the gas flux is achieved when 1% of AWCs are incorporated.

3.3 Membranes performance in DCMD

The choice of the optimal membranes was based on their intrinsic properties such that it satisfies the requirements for effective MD performances as published in literature (Table 3).

To be applied to MD experiments, the membranes should possess at least one hydrophobic layer to avoid wettability of the feed solution (Eykens et al., 2016). In addition, they should present a sufficient LEP_W that is achieved by pore dimensions ranging from several nanometers to a maximum of 0.5 μm (Khayet, 2011). Finally, a compromise must be found between a high mechanical strength and a high porosity of the hydrophobic layer (Phattaranawik et al., 2003; Eykens et al., 2016).

Among all the characterizations and collected data, two stand out membranes could be singled out, notably membrane M0-a and its corresponding HC6-modified membrane M1-a, whose characteristics are listed in Table 4.

Each set of DCMD experiment was carried out during 3 h, giving a NaCl rejection rate of 85.2% for the reference M0-a membrane and 95.3% for the hybrid M1-a membrane. Permeate flux values are reported for some commercial membranes (PVDF Millipore and Pall) and examples of hybrid PVDF membranes, as reported in the literature (PVDF/MWCNT and PVDF/CNT). These results are in accordance with the pure water permeability characterization results whereby the HC6-modified membrane displayed a higher water permeability than its reference PVDF membrane. While these two processes are two different methods, the results observed in each configuration seem to corroborate and tend to point towards the influence of a given weight percentage of HC6 within the polymeric matrix.

Our results were compared to the literature in Table 5 and appear to be very promising since a permeate flux at least four times higher was obtained even with the reference membrane M0-a.

TABLE 5 Comparison of the permeate flux obtained in this study with the literature for DCMD process.

Membrane	Permeate flux (kg/m^{2}h)	Ref
PVDF (GVHP, Millipore)	10.37	Phattaranawik et al. (2003)
PVDF (HVHP, Millipore)	11.67	Phattaranawik et al. (2003)
PVDF (Millipore Sigma)	37.4	Silva et al. (2015)
PVDF (Pall)	23.2	Puranik et al. (2019)
PVDF (HVHP, Millipore)	17	Eykens et al. (2017)
PVDF/MWCNT	34.2	Silva et al. (2015)
PVDF/CNT (CNIM)[a]	51.4	Ragunath et al. (2018)
M0-a	48.91	This study
M1-a	54.09	This study

[a]PVDF/CNT (CNIM): Carbon nanotube immobilized membrane.

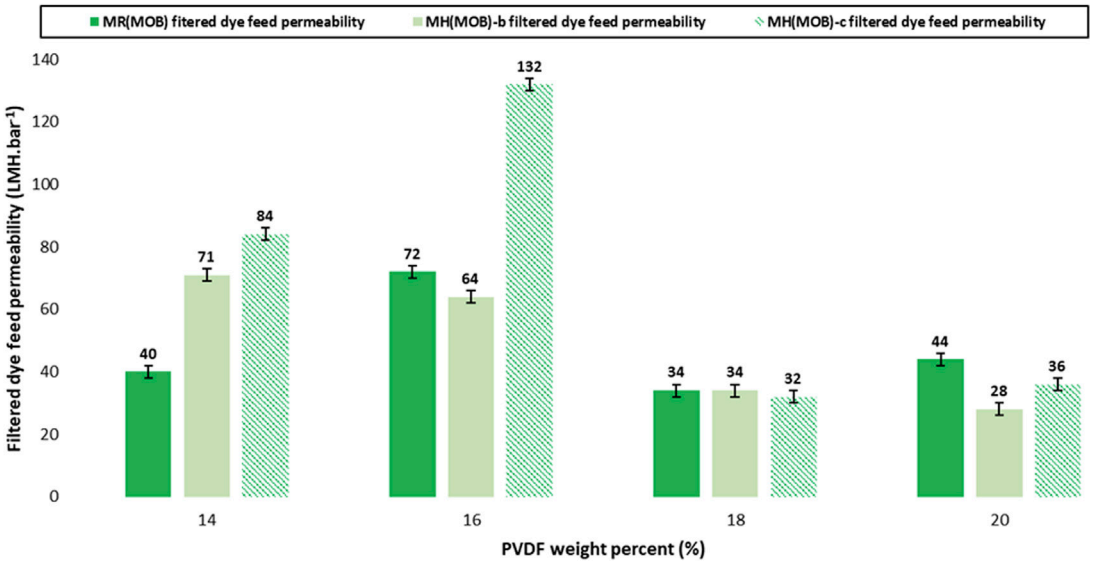

FIGURE 9
Filtered MO-MB feed permeability of PVDF reference membranes—MR (MOB), of 0.05 wt% HC6 modified membranes—MH(MOB)-b series, and of 0.075 wt% HC6 modified membranes—MH(MOB)-c series (MW 530,000 g/mol) with binary dye mixtures of MO-MB. Operating conditions: 3 bar transmembrane pressure, room temperature (20°C ± 2°C), Operating conditions: 3 bar transmembrane pressure, room temperature (20°C ± 2°C), mixed dye solution with a total concentration of 20 mg/L and concentration ratio of 1:1.

3.4 Membranes performance in ultrafiltration of single dyes and binary dyes mixtures

3.4.1 Single dyes separation

The filtration performance (filtered dye feed permeability and dye feed rejection efficiency) of reference PVDF M0-a membrane and of HC6-modified M1-a membrane were investigated for single dyes, namely, anionic methyl orange (MO) and cationic methylene blue (MB). Compared to the pure water permeability, a decrease in the permeability of the filtered dye feed was observed in the case of each single dye. This typical phenomenon of the filtration process could be due to the effect of concentration polarization and adsorption of dye molecules on the membrane surface (Kumar and Ismail, 2015). The filtered dye feed permeability of the HC6-modified membrane was improved as compared to the PVDF reference membrane. However, this improvement in the permeability was offset by the low rejection efficiency between 70%–85%) observed for the HC6-modified membranes.

3.4.2 Binary dyes mixtures separation

The filtration performances of the prepared membranes were further assessed for two binary dyes mixtures. The first binary system

consisted of MO and MB, noted MOB in Supplementary Table S2. It was found that both the rejection efficiency and the filtered dye feed permeability of the anionic-cationic dye mixture were improved as compared to those of the single dye feeds, notably methyl orange (Figure 9). While the complete removal of methylene blue (MB) was achieved with the reference membranes, the rejection efficiency of methyl orange in the binary mixture was improved up to 99%. We observe a minimal variation of the values for the rejection 96%–99% which are considered as very good performances for the separation of dyes (Figure 10) It is suggested that the electrostatic interaction between the two oppositely charged dyes could play an essential role in the highly improved net rejection efficiency of the dyes mixture. A second binary system consisting of negatively co-charged dyes, namely, Methyl Orange and Eriochrome Black T was hence investigated to evaluate whether the dye electrostatic charge effect along with the incorporation of HC6 could indeed play an essential role on the filtration performance of the PVDF reference membranes and of their HC6-modified membranes. We can also note that the rejection efficiency of the binary mixture of the co-charged dyes is much lower than that yielded by the binary mixture of the oppositely charged dyes. While the filtered dye feed permeability of the HC6 modified membranes has been improved in most cases as compared to their reference membranes, the rejection efficiency was nowhere near to those of the binary mixture of the oppositely charged dyes.

4 Conclusion

We synthesized a new series of PVDF and PVDF-AWC hybrid membranes using a polymer grade of 530,000 g/mol. The physico-chemical characterizations of the HC6-modified membrane confirmed the successful incorporation of the AWC within the polymeric matrix which is composed of hydrophilic networks of PVDF core-AWC surface hybrid nanoparticules. These innovative original strategies in which water channels structures contribute to water cluster stabilization and the increase of water (vapors or liquid) within hydrophobic pore structures may indeed be used to prepare PVDF MD and UF membranes for enhanced separations. ATG/DSC and XRD analyses allowed for the observation of new hybrid phases. In addition, the influence of the HC6 content within the polymer matrix was studied and an optimal value of 0.05 wt% was noticed to give a good compromise between the porosity, the hydrophobicity, the LEP_W and the pure water permeability.

In addition, the most improved water permeability (by a factor 2.45) was reached for the M1-a membrane containing 0.05 wt% of HC6 compared to the reference PVDF membrane, M0-a and a higher flux than those reported in the literature. While the salt rejection of the HC6- modified membrane is lower than 99%, it should be noted that no other additives apart from the amphiphilic AWCs were used for the preparation of the hybrid membranes. This provides further scope to improve the HC6-modified membrane by blending with other constituents. The membranes will also be tested in air gap membrane distillation configuration to better evaluate the performance of our proposed membranes.

The polymeric membranes displayed good filtration performance for dye removal application. An anionic-cationic dyes mixture of methyl orange and of methylene blue proved to offer a net improvement on the filtration performance of both types of membranes, namely, reference membrane MR (MOB)-1 and HC6-modified membrane MH(MOB)-1c. While the binary mixture allowed for the complete removal of methylene blue, the rejection efficiency of methyl orange was improved as compared to when they were used in their single forms. The filtered dye feed permeability of MR (MOB)-1 was improved by a factor of 2.1, further indicating the presence of HC6 within the polymeric matrix. The study revealed that the electrostatic interaction between the two oppositely charged dyes improved the net rejection efficiency of the binary dye mixture.

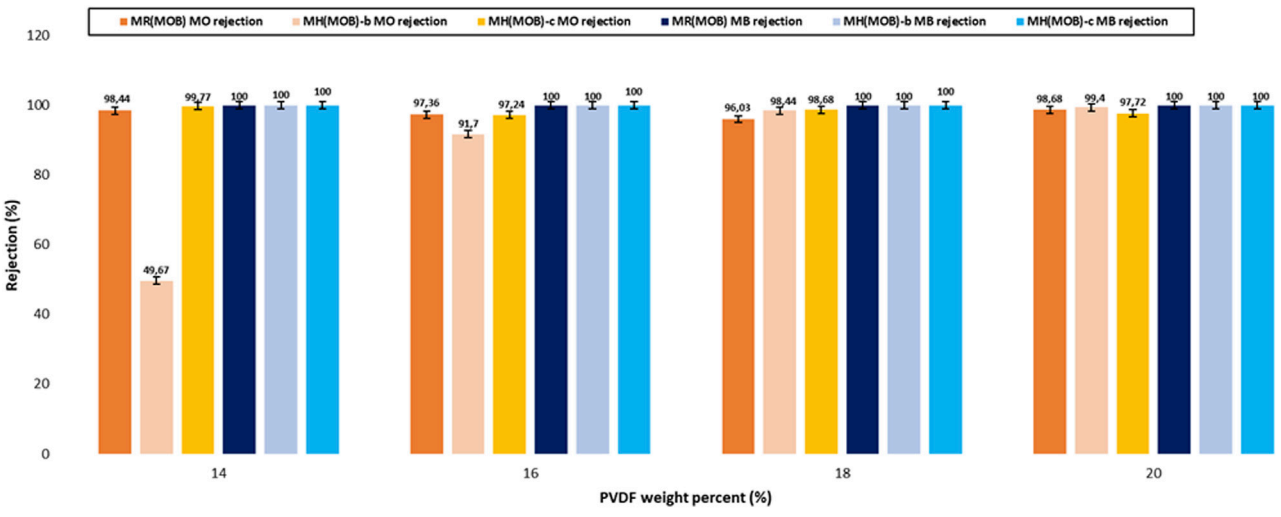

FIGURE 10
Dye rejection of PVDF reference membranes—MR (MOB) series, of 0.05 wt% HC6 modified membranes—MH(MOB)-b series and of 0.075 wt% HC6 modified membranes—MH(MOB)-c series (MW 530,000 g/mol) with binary dye mixtures of MO-MB. Operating conditions: 3 bar transmembrane pressure, room temperature (20°C ± 2°C), mixed dye solution with a total concentration of 20 mg/L and concentration ratio of 1:1.

Data availability statement

The original contributions presented in the study are included in the article/Supplementary Material, further inquiries can be directed to the corresponding authors.

Author contributions

MB, SC, and KN contributed to conception and design of the study. KN carried out the experimental work and organized the database. V-EM performed the SEM and STEM characterization. KN wrote the first draft of the manuscript. MB and SC critically reviewed and organized the manuscript. All authors contributed to the article and approved the submitted version.

Funding

This project has received funding from the European Union's Horizon 2020 research and innovation programme under grant agreement INTELWAT No 958454.

Conflict of interest

The authors declare that the research was conducted in the absence of any commercial or financial relationships that could be construed as a potential conflict of interest.

Publisher's note

All claims expressed in this article are solely those of the authors and do not necessarily represent those of their affiliated organizations, or those of the publisher, the editors and the reviewers. Any product that may be evaluated in this article, or claim that may be made by its manufacturer, is not guaranteed or endorsed by the publisher.

Supplementary material

The Supplementary Material for this article can be found online at: https://www.frontiersin.org/articles/10.3389/frmst.2023.1241526/full#supplementary-material

References

Adnan, S., Hoang, M., Wang, H., and Xie, Z. (2012). Commercial PTFE membranes for membrane distillation application: effect of microstructure and support material. *Desalination* 284, 297–308. doi:10.1016/j.desal.2011.09.015

Ahmad, N. A., Leo, C. P., Ahmad, A. L., and Ramli, W. K. W. (2015). Membranes with great hydrophobicity: a review on preparation and characterization. *Sep. Purif. Rev.* 44, 109–134. doi:10.1080/15422119.2013.848816

Akbari, A., Hamadanian, M., Jabbari, V., Lehi, A. Y., and Bojaran, M. (2012). Influence of PVDF concentration on the morphology, surface roughness, crystalline structure, and filtration separation properties of semicrystalline phase inversion polymeric membranes. *Desalination Water Treat.* 46, 96–106. doi:10.1080/19443994.2012.677524

Amini, M., Arami, M., Mahmoodi, N. M., and Akbari, A. (2011). Dye removal from colored textile wastewater using acrylic grafted nanomembrane. *Desalination* 267, 107–113. doi:10.1016/j.desal.2010.09.014

Aquino, R. R., Tolentino, M. S., Angeles, J., and Millano, H. A. (2018). Fabrication and characterization of electrospun polysulfone (PSF)/Organo-Montmorillonite (O-mmt) nanostructured membranes. *Mater. Sci. Forum* 916, 125–129. doi:10.4028/www.scientific.net/msf.916.125

Chamani, H., Woloszyn, J., Matsuura, T., Rana, D., and Lan, C. Q. (2021). Pore wetting in membrane distillation: a comprehensive review. *Prog. Mater. Sci.* 122, 100843. doi:10.1016/j.pmatsci.2021.100843

Chang, H., Liu, B., Zhang, Z., Pawar, R., Yan, Z., Crittenden, J. C., et al. (2021). A critical review of membrane wettability in membrane distillation from the perspective of interfacial interactions. *Environ. Sci. Technol.* 55, 1395–1418. doi:10.1021/acs.est.0c05454

Chen, X., Zhao, Y., Moutinho, J., Shao, J., Zydney, A. L., and He, Y. (2015). Recovery of small dye molecules from aqueous solutions using charged ultrafiltration membranes. *J. Hazard. Mater.* 284, 58–64. doi:10.1016/j.jhazmat.2014.10.031

Chuang, W.-Y., Young, T.-H., Chiu, W.-Y., and Lin, C.-Y. (2000). The effect of polymeric additives on the structure and permeability of poly(vinyl alcohol) asymmetric membranes. *Polymer* 41, 5633–5641. doi:10.1016/s0032-3861(99)00818-6

Cui, Z., Drioli, E., and Lee, Y. M. (2014). Recent progress in fluoropolymers for membranes. *Prog. Polym. Sci.* 39, 164–198. doi:10.1016/j.progpolymsci.2013.07.008

Darvishmanesh, S., Jansen, J. C., Tasselli, F., Tocci, E., Luis, P., Degrève, J., et al. (2011). Novel polyphenylsulfone membrane for potential use in solvent nanofiltration. *J. Membr. Sci.* 379, 60–68. doi:10.1016/j.memsci.2011.05.045

Dasgupta, J., Sikder, J., Chakraborty, S., Curcio, S., and Drioli, E. (2015). Remediation of textile effluents by membrane based treatment techniques: a state of the art review. *J. Environ. Manag.* 147, 55–72. doi:10.1016/j.jenvman.2014.08.008

Di Vincenzo, M., Tiraferri, A., Musteata, V., Chisca, S., Sougrat, R., Huang, L., et al. (2021). Biomimetic artificial water channel membranes for enhanced desalination. *Nat. Nanotechnol.* 16, 190–196. doi:10.1038/s41565-020-00796-x

Drioli, E., Ali, A., and Macedonio, F. (2015). Membrane distillation: recent developments and perspectives. *Desalination* 356, 56–84. doi:10.1016/j.desal.2014.10.028

El-Bourawi, M. S., Ding, Z., Ma, R., and Khayet, M. (2006). A framework for better understanding membrane distillation separation process. *J. Membr. Sci.* 285, 4–29. doi:10.1016/j.memsci.2006.08.002

Eykens, L., De Sitter, K., Dotremont, C., Pinoy, L., and Van der Bruggen, B. (2017). Membrane synthesis for membrane distillation: a review. *Sep. Purif. Technol.* 182, 36–51. doi:10.1016/j.seppur.2017.03.035

Eykens, L., De Sitter, K., Dotremont, C., Pinoy, L., and Van der Bruggen, B. (2016). How to optimize the membrane properties for membrane distillation: a review. *Ind. Eng. Chem. Res.* 55, 9333–9343. doi:10.1021/acs.iecr.6b02226

Fadhil, S., Marino, T., Makki, H. F., Alsalhy, Q. F., Blefari, S., Macedonio, F., et al. (2016). Novel PVDF-HFP flat sheet membranes prepared by triethyl phosphate (TEP) solvent for direct contact membrane distillation. *Chem. Eng. Process. Process Intensif.* 102, 16–26. doi:10.1016/j.cep.2016.01.007

Guillen, G. R., Pan, Y., Li, M., and Hoek, E. M. V. (2011). Preparation and characterization of membranes formed by nonsolvent induced phase separation: a review. *Ind. Eng. Chem. Res.* 50, 3798–3817. doi:10.1021/ie101928r

Hamzah, N., and Leo, C. P. (2016). Fouling prevention in the membrane distillation of phenolic-rich solution using superhydrophobic PVDF membrane incorporated with TiO2 nanoparticles. *Sep. Purif. Technol.* 167, 79–87. doi:10.1016/j.seppur.2016.05.005

Hsu, S. T., Cheng, K. T., and Chiou, J. S. (2002). Seawater desalination by direct contact membrane distillation. *Desalination* 143, 279–287. doi:10.1016/s0011-9164(02)00266-7

Hui Ting, L. L., Teow, Y. H., Mahmoudi, E., and Ooi, B. S. (2023). Development and optimization of low surface free energy of rGO-PVDF mixed matrix membrane for membrane distillation. *Sep. Purif. Technol.* 305, 122428. doi:10.1016/j.seppur.2022.122428

Julian, H., Sutrisna, P. D., Hakim, A. N., Harsono, H. O., Hugo, Y. A., and Wenten, I. G. (2019). Nano-silica/polysulfone asymmetric mixed-matrix membranes (MMMs) with high CO2 permeance in the application of CO2/N2 separation. *Polymer-Plastics Technol. Mater.* 58, 678–689. doi:10.1080/03602559.2018.1520253

Kang, G., and Cao, Y. (2014). Application and modification of poly(vinylidene fluoride) (PVDF) membranes – a review. *J. Membr. Sci.* 463, 145–165. doi:10.1016/j.memsci.2014.03.055

Khayet, M., Cojocaru, C., and García-Payo, M. C. (2010). Experimental design and optimization of asymmetric flat-sheet membranes prepared for direct contact membrane distillation. *J. Membr. Sci.* 351, 234–245. doi:10.1016/j.memsci.2010.01.057

Khayet, M. (2011). Membranes and theoretical modeling of membrane distillation: a review. *Adv. Colloid Interface Sci.* 164, 56–88. doi:10.1016/j.cis.2010.09.005

Kim, J., Kim, J., Lee, Y. M., and Drioli, E. (2015). Thermally induced phase separation and electrospinning methods for emerging membrane applications: a review. *AIChE J.* 62, 461–490. doi:10.1002/aic.15076

Kim, S., Heath, D. E., and Kentish, S. E. (2023). Crosshatched nanofibre membranes for direct contact membrane distillation. *Desalination* 548, 116277. doi:10.1016/j.desal.2022.116277

Kumar, R., and Ismail, A. (2015). Fouling control on microfiltration/ultrafiltration membranes: effects of morphology, hydrophilicity, and charge. *J. Appl. Polym. Sci.* 132. doi:10.1002/app.42042

Kumar, S., Terashima, C., Fujishima, A., Krishnan, V., and Pitchaimuthu, S. (2019). "Photocatalytic degradation of organic pollutants in water using graphene oxide composite," in *A new generation material graphene: applications in water Technology*. Editor Mu Naushad (Cham, Germany: Springer International Publishing), 413–438.

Le Duc, Y., Michau, M., Gilles, A., Gence, V., Legrand, Y.-M., Lee, A., et al. (2011). Imidazole-quartet water and proton dipolar channels. *Angewandte Chemie Int. ed. Engl.* 50, 11366–11372. doi:10.1002/anie.201103312

Lin, Q., Gao, M., Chang, J., and Ma, H. (2016). Adsorption properties of crosslinking carboxymethyl cellulose grafting dimethyldiallylammonium chloride for cationic and anionic dyes. *Carbohydr. Polym.* 151, 283–294. doi:10.1016/j.carbpol.2016.05.064

Liu, F., Hashim, N. A., Liu, Y., Abed, M. R. M., and Li, K. (2011). Detectable expression of IL-35 in CD4+ T cells from peripheral blood of chronic hepatitis B patients. *J. Membr. Sci.* 375, 1–5. doi:10.1016/j.clim.2010.12.012

Lu, H., Wang, J., Wang, T., Wang, N., Bao, Y., and Hao, H. (2017). Crystallization techniques in wastewater treatment: an overview of applications. *Chemosphere* 173, 474–484. doi:10.1016/j.chemosphere.2017.01.070

Machado, P. S. T., Habert, A. C., and Borges, C. P. (1999). Membrane formation mechanism based on precipitation kinetics and membrane morphology: flat and hollow fiber polysulfone membranes. *J. Membr. Sci.* 155, 171–183. doi:10.1016/s0376-7388(98)00266-x

Minitha, C. R., Lalitha, M., Jeyachandran, Y. L., Senthilkumar, L., and Rajendra Kumar, R. T. (2017). Adsorption behaviour of reduced graphene oxide towards cationic and anionic dyes: co-action of electrostatic and π – π interactions. *Mater. Chem. Phys.* 194, 243–252. doi:10.1016/j.matchemphys.2017.03.048

Mulder, M. (1996). *Basic principles of membrane Technology*. Netherlands: Springer.

Nguyen, T. A., and Juang, R.-S. (2013). Treatment of waters and wastewaters containing sulfur dyes: a review. *Chem. Eng. J.* 219, 109–117. doi:10.1016/j.cej.2012.12.102

Nikooe, N., and Saljoughi, E. (2017). Preparation and characterization of novel PVDF nanofiltration membranes with hydrophilic property for filtration of dye aqueous solution. *Appl. Surf. Sci.* 413, 41–49. doi:10.1016/j.apsusc.2017.04.029

Pal, P. (2015). Arsenic removal by membrane distillation. *Int. J. Eng. Res. Technol. (IJERT)* 1, 179–270. doi:10.1016/B978-0-12-801281-9.00005-9

Pendergast, M. M., and Hoek, E. M. V. (2011). A review of water treatment membrane nanotechnologies. *Energy Environ. Sci.* 4, 1946–1971. doi:10.1039/c0ee00541j

Phattaranawik, J., Jiraratananon, R., and Fane, A. G. (2003). Effect of pore size distribution and air flux on mass transport in direct contact membrane distillation. *J. Membr. Sci.* 215, 75–85. doi:10.1016/s0376-7388(02)00603-8

Pramanik, B. K., Thangavadivel, K., Shu, L., and Jegatheesan, V. (2016). A critical review of membrane crystallization for the purification of water and recovery of minerals. *Rev. Environ. Sci. Bio/Technology* 15, 411–439. doi:10.1007/s11157-016-9403-0

Puranik, A. A., Rodrigues, L. N., Chau, J., Li, L., and Sirkar, K. K. (2019). Porous hydrophobic-hydrophilic composite membranes for direct contact membrane distillation. *J. Membr. Sci.* 591, 117225. doi:10.1016/j.memsci.2019.117225

Ragunath, S., Roy, S., and Mitra, S. (2018). Carbon nanotube immobilized membrane with controlled nanotube incorporation via phase inversion polymerization for membrane distillation based desalination. *Sep. Purif. Technol.* 194, 249–255. doi:10.1016/j.seppur.2017.11.053

Roshani, R., Ardeshiri, F., Peyravi, M., and Jahanshahi, M. (2018). Highly permeable PVDF membrane with PS/ZnO nanocomposite incorporated for distillation process. *RSC Adv.* 8, 23499–23515. doi:10.1039/c8ra02908c

Shaban, M., Abukhadra, M. R., Ibrahim, S. S., and Shahien, M. G. (2017). Photocatalytic degradation and photo-Fenton oxidation of Congo red dye pollutants in water using natural chromite—response surface optimization. *Appl. Water Sci.* 7, 4743–4756. doi:10.1007/s13201-017-0637-y

Sharma, K., Dalai, A. K., and Vyas, R. K. (2018). Removal of synthetic dyes from multicomponent industrial wastewaters. *Rev. Chem. Eng.* 34, 107–134. doi:10.1515/revce-2016-0042

Silva, T. L. S., Morales-Torres, S., Figueiredo, J. L., and Silva, A. M. T. (2015). Multi-walled carbon nanotube/PVDF blended membranes with sponge- and finger-like pores for direct contact membrane distillation. *Desalination* 357, 233–245. doi:10.1016/j.desal.2014.11.025

Srivastava, H. P., Arthanareeswaran, G., Anantharaman, N., and Starov, V. M. (2011). Performance of modified poly(vinylidene fluoride) membrane for textile wastewater ultrafiltration. *Desalination* 282, 87–94. doi:10.1016/j.desal.2011.05.054

Tai, Z. S., Othman, M. H. D., Koo, K. N., and Jaafar, J. (2023). Critical review on membrane designs for enhanced flux performance in membrane distillation. *Desalination* 553, 116484. doi:10.1016/j.desal.2023.116484

Tan, X., and Rodrigue, D. (2019). A Review on Porous Polymeric Membrane Preparation. Part I: production techniques with polysulfone and poly (vinylidene fluoride). *Polymers* 11, 1160. doi:10.3390/polym11071160

Tarvainen, T., Svarfvar, B., Åkerman, S., Savolainen, J., Karhu, M., Paronen, P., et al. (1999). Drug release from a porous ion-exchange membrane *in vitro*. *Biomaterials* 20, 2177–2183. doi:10.1016/s0142-9612(99)00122-2

Tomaszewska, M. (1996). Preparation and properties of flat-sheet membranes from poly(vinylidene fluoride) for membrane distillation. *Desalination* 104, 1–11. doi:10.1016/0011-9164(96)00020-3

Ulbricht, M. (2006). Advanced functional polymer membranes. *Polymer* 47, 2217–2262. doi:10.1016/j.polymer.2006.01.084

van de Witte, P., Dijkstra, P. J., van den Berg, J. W. A., and Feijen, J. (1996). Phase separation processes in polymer solutions in relation to membrane formation. *J. Membr. Sci.* 117, 1–31. doi:10.1016/0376-7388(96)00088-9

Wang, D.-M., and Lai, J.-Y. (2013). Recent advances in preparation and morphology control of polymeric membranes formed by nonsolvent induced phase separation. *Curr. Opin. Chem. Eng.* 2, 229–237. doi:10.1016/j.coche.2013.04.003

Wang, P., and Chung, T.-S. (2015). Recent advances in membrane distillation processes: membrane development, configuration design and application exploring. *J. Membr. Sci.* 474, 39–56. doi:10.1016/j.memsci.2014.09.016

Yi, Z., Zhu, L.-P., Zhao, Y.-F., Zhu, B.-K., and Xu, Y.-Y. (2012). An extending of candidate for the hydrophilic modification of polysulfone membranes from the compatibility consideration: the polyethersulfone-based amphiphilic copolymer as an example. *J. Membr. Sci.* 390–391, 48–57. doi:10.1016/j.memsci.2011.10.058

Zhao, Y.-F., Zhu, L.-P., Yi, Z., Zhu, B.-K., and Xu, Y.-Y. (2013). Improving the hydrophilicity and fouling-resistance of polysulfone ultrafiltration membranes via surface zwitterionicalization mediated by polysulfone-based triblock copolymer additive. *J. Membr. Sci.* 440, 40–47. doi:10.1016/j.memsci.2013.03.064

Zhou, L., Zhang, H., Ahmad, A. L., Tan, S. H., Low, S. C., and Li, C. (2023). Hierarchical structure design of electrospun membrane for enhanced membrane distillation treatment of shrimp aquaculture wastewater. *Sep. Purif. Technol.* 306, 122591. doi:10.1016/j.seppur.2022.122591